Contents lists available at ScienceDirect

Journal of Inorganic Biochemistry





Interactions of arylhydroxylamines and alkylaldoximes with a rhodium porphyrin

Jennifer Londoño-Salazar, Megan Ayala, Douglas R. Powell, Yihan Shao*, George B. Richter-Addo*

Department of Chemistry and Biochemistry, University of Oklahoma, Norman, Oklahoma 73019, USA

ARTICLE INFO

Keywords:
Hydroxylamine
Aldoxime
X-ray structure
DFT calculation
Intramolecular H-bond
Porphyrin
Rhodium

ABSTRACT

Heme enzymes are involved in the binding and metabolism of hydroxylamine (RNHOH) and aldoxime (RCH=NOH) compounds (R = H, alkyl, aryl). We report the synthesis and X-ray crystal structure of a metalloporphyrin in complex with an arylhydroxylamine, namely that of (TPP)Rh(PhNHOH)(C_6H_4 Cl) (TPP = tetraphenylpophryinato dianion). The crystal structure reveals, in addition to N-binding of PhNHOH to Rh, the presence of an intramolecular H-bond between the hydroxylamine –OH proton and a porphyrin N-atom. Results from density functional theory (DFT) calculations support the presence of this intramolecular H-bond in this global minimum structure, and a natural bond order (NBO) analysis reveals that this H-bond comprises a donor π N=C (porphyrin) to acceptor σ^* O-H (hydroxylamine) interaction of 2.32 kcal/mol. While DFT calculations predict the presence of similar intramolecular H-bond interactions in the related aldoxime complexes (TPP)Rh (RCH=NOH)(C_6H_4 Cl) in their global minima structures, the X-ray crystal structure obtained for the (TPP)Rh (CH₃(CH₂)₂CH=NOH)(C_6H_4 Cl) complex is consistent with the local (non-global) minima conformation that does not have this intramolecular H-bond interaction.

1. Introduction

Organic compounds containing the N-hydroxyl "NOH" functional group are important intermediates in the global nitrogen cycle. Examples of compounds that include this moiety include N-hydroxylamines and aldoximes (Fig. 1).

The simplest hydroxylamine, namely NH₂OH, is a natural substrate for the multiheme enzyme hydroxylamine oxidoreductase (HAO) [1–3], and has been identified as an intermediate in enzymatic nitrite reduction [4] and hydrazine synthesis [5]. The N-binding mode of NH₂OH appears to be the dominant feature of its binding to the Fe centers of heme proteins for the cases where direct binding has been established by crystallography [2,4,6,7]. The direct N-binding of NH₂OH to cytochrome c' has recently been established using resonance Raman spectroscopy employing ^{15}N -isotopic labeling [8]. Alkyl/arylhydroxylamines (RNHOH) have also been identified as biological intermediates during the oxidative metabolism of amines (RNH₂)

[9–13], and similar to what is observed with the parent NH_2OH , the RNHOH metabolites may interact directly with Fe heme centers.

Oximes play important roles in biology as well. For example, aldoximes such as 2-methylbutyraldoxime and phenylacetaldoxime have been identified in plants, and several of such oximes have been implicated in plant metabolism associated with growth regulation, defense, pollinator attraction, and plant communication with the environment [14], Recently, a new class of heme-containing enzymes that catalyze the dehydration of aldoximes to nitriles (Fig. 2) have been identified [15–17]. These enzymes have been named aldoxime dehydratases (Oxd), and several of these Oxd enzymes have now been discovered in bacteria and fungi [18]. In these enzymes, the aldoxime substrates bind directly to the heme Fe centers as determined by X-ray crystallography of enzyme-substrate complexes, where the substrates in these cases are propionaldoxime, butyraldoxime, and 2-(3-bromophenyl)propanaldoxime [19,20]. It has been shown that N-binding of the oxime to ferrous hemes leads to nitrile production, whereas the O-

E-mail addresses: yihan.shao@ou.edu (Y. Shao), grichteraddo@ou.edu (G.B. Richter-Addo).

^{*} Corresponding authors.

Fig. 1. Sketches of *N*-hydroxylamines and aldoximes (R = H, alkyl, or aryl).

Fig. 2. The reaction catalyzed by heme-containing aldoxime dehydratase (Oxd) enzymes.

binding mode in ferric derivatives is inactive for the reaction [21]. Interestingly, this heme-dependent enzymatic route for the aldoxime-to-nitrile conversion reaction has provided an attractive and convenient entry into a "green" alternative for the industrially important nitrile synthesis from aldoximes [18].

We are interested in determining the structural and electronic factors involved in the binding of organo-NHxOy complexes to synthetic metalloporphyrins. We recently reported the synthesis and X-ray crystal structures of synthetic metalloporphyrin complexes of the first-row transition metals Fe and Co with N-hydroxyamphetamine (AmphN-HOH), in which hitherto unrecognized intramolecular H-bonds were present between the hydroxylamines and porphyrin N-atoms (left of Fig. 3) [22]. Mansuy [23] and Chi-Ming Che [24] have reported the preparation of the related unstable heme model (porphyrin)Fe(i-PrNHOH)(i-PrNO) and (porphyrin)Ru(PhNHOH)(PhNO) complexes, respectively, although the -NHOH conformations were not structurally determined. We showed, using natural bond order analyses, that the intramolecular H-bonds observed in our Fe- and Co-AmphNHOH derivatives involved porphyrin π to σ^* (O–H) interactions weakened the O-H bonds. In addition, we [22] and others [25,26] have shown through computational calculations that such intramolecular H-bonds are also possible for the related heme-H2O2 interactions, although to our knowledge they have not to date been observed experimentally for H₂O₂

Given that heme model-alkylhydroxylamine complexes can display this intramolecular H-bond interaction [22], we have extended our examination of this chemical space involving related and geometrically-aligned M–X–O–H–Np systems (right of Fig. 3; Np = porphyrin N-atom) to determine if such intramolecular H-bond interactions are also possible for second-row transition metals (e.g., M = Rh in this work), arylhydroxylamines (X = ArNH), and for aldoximes (X = RCH=N). In this article, we report the first crystal structures of a hydroxylamine and an aldoxime to a Rh porphyrin. We employ DFT calculations to show that such intramolecular H-bond interactions represent, in the absence of competing environmental effects, global minima along their potential energy curves. The experimental X-ray crystal structure of the Rh-arylhydroxylamine adduct reveals this intramolecular H-bond, but that of the Rh-aldoxime complex obtained in this current work does not.

2. Results and discussion

2.1. Preparation and Molecular Structure of (TPP)Rh(PhNHOH) (C₆H₄Cl)

The air-sensitive target compound (TPP)Rh(PhNHOH)(C_6H_4Cl) (TPP = tetraphenylporphyrinato dianion) was obtained from the reaction of the five-coordinate rhodium precursor (TPP)Rh(C_6H_4Cl) in CH_2Cl_2 at room temperature with excess phenylhydroxylamine (PhNHOH) under anaerobic conditions (top of Scheme 1). The dark red crystalline product was obtained in 61% isolated yield after workup.

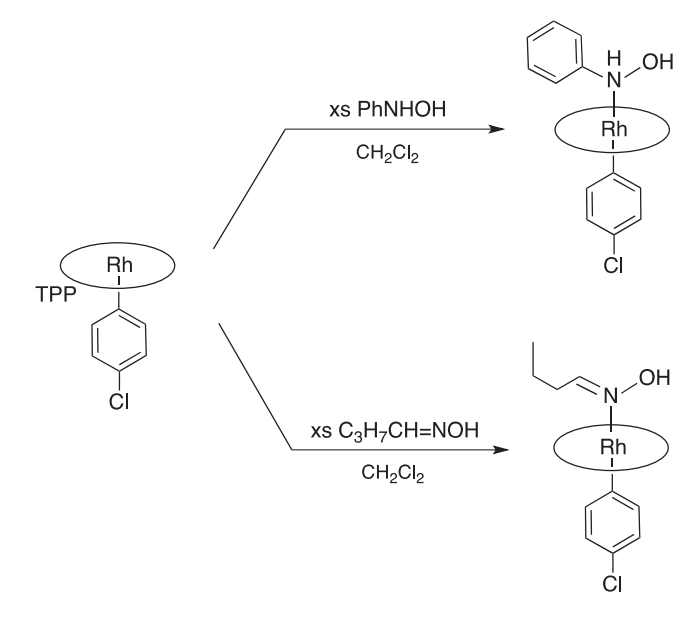
The IR spectrum of the product as a KBr pellet displayed a band at 1074 cm^{-1} assigned to υ_{NO} based on comparison with the computed

Fig. 3. Schematic of the (*left*) observed intramolecular H-bond between bound N-hydroxyamphetamine and Fe^{II} and Co^{II} porphyrins, (*middle*) calculated intramolecular H-bond interaction between bound H_2O_2 and $Fe^{II/III}$ porphyrins, and (*right*) goals of this work where M = Rh and X = PhNH or RCH = N. [Np = porphyrin N-atom].

spectrum (Supporting Information Figs. S2-S3). We note that Luckhuaus identified the υ_{NO} of free NH₂OH at 895.21 cm $^{-1}$ using its rovibrational spectrum [27], which is close to the value of 899.9 cm $^{-1}$ obtained by Withnall and Andrews using the vibrational spectra of matrix-isolated NH₂OH and its $^{15}N, \, ^{18}O$ and deuterium substituted isotopomers [28]. Coordination compounds of the parent NH₂OH typically display $\upsilon_{NO}s$ in the 985–932 cm $^{-1}$ region [29], although values up to 1035 cm $^{-1}$ have been reported (cited in [8]). Resonance Raman measurements on a ferrous-NH₂OH cytochrome \emph{c} ' reveal a υ_{NO} at 906 cm $^{-1}$ [8].

The identity of the product (top of Scheme 1) was established by X-ray crystallography which confirmed the six-coordination around the Rh center (Fig. 4). The O1 atom of the axial PhNHOH ligand exhibits a 70:30 disorder (the bound N5 atom is not disordered), and the *p*-Cl atom of the axial aryl halide ligand is also disordered (89:11, *p-:m-*; Supporting Information Fig. S4). The major components for this structure are shown in the figure, with selected bond lengths and angles shown in the caption.

The PhNHOH ligand is *N*-bound to the formally Rh(III) center. The axial Rh1–N5 bond length of 2.300(4) Å is slightly longer than those determined in other six-coordinate Rh(III) porphyrin complexes; e.g., (TPP)Rh(*N*-MeIm)Cl (2.058(2) Å) [30] and (TPP)Rh(py)Cl (2.075(6) Å) [31]. The *trans* axial Rh1–C51 bond length of 2.010(4) Å is similar to that reported for the six-coordinate (TTP)Rh(MeOH)(C_6H_4Br -p) (2.028 (8) Å) [32] and within the range of five-coordinate organo-Rh(III) porphyrin complexes; e.g., (TPP)Rh(Ph) (1.984(6) Å) [33] and (TTP)Rh



Scheme 1. Preparation of the hydroxylamine (top) and oxime (bottom) complexes.

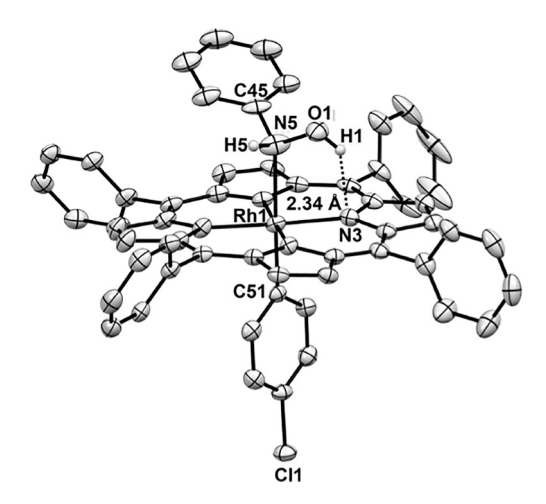


Fig. 4. Molecular structure of (TPP)Rh(PhNHOH)(C_6H_4CI); major component shown. The two H atoms of the –NHOH moiety (i.e., H1 and H5) were located in the difference electron density map and were refined independently. The H-bond between the porphyrin N3 atom and the NOH proton (H1) is represented by a dashed line (N3 $^{-}$ H1 = 2.34 Å). The other H atoms have been removed for clarity. Thermal ellipsoids are drawn at 50%. Selected bond lengths (A) and angles (°): Rh1–N5 = 2.300(4), N5–O1 = 1.336(6) [1.337(7)], C45–N5 = 1.433 (7), Rh1–C51 = 2.010(4), Rh1–N(por) = 2.025(4)-2.036(4), \angle Rh1–N5–O1 = 113.6(3) [122.1(6)], \angle Nh1–N5–C45 = 118.1(3), \angle C45–N5–O1 = 111.0(5) [115.0(6)], \angle N5–Rh–C51 = 177.78(18). Data involving the disordered O1 (30%) atom are in brackets.

(C₆H₄Cl-p) (2.138(6) Å) [32].

Importantly, the hydroxyl proton of the phenylhydroxylamine –NHOH moiety is engaged in a H-bonding interaction with a porphyrin N-atom (dashed line in Fig. 4). Interestingly, in the case of the minor (30%) disordered component involving the O-atom, the orientation of the hydroxyl proton is such that it points "upward" and is not engaged in such a H-bond (Fig. S4 in the Supporting Information).

Occurrence of both orientations of the –NHO*H* proton in the crystal structure to either involve the intramolecular H-bond with a porphyrin N-atom (major component) or not (minor component) prompted us to further examine this H-bonding feature using density functional theory (DFT) calculations.

2.2. Computational insights

2.2.1. Geometry optimization

The X-ray structural coordinates of the major disordered component of the structure were utilized as the starting structure in the computed geometry optimization. The resulting optimized structure from the DFT calculations was in excellent agreement with the major component in the X-ray structure (RMSD of 0.2055 Å), with the –NHOH hydroxyl proton pointing in a direction to engage in the intramolecular H-bond with a porphyrin N-atom (Fig. S5 in the Supporting Information). The largest deviations in the computed versus experimental structures were in the porphyrin's peripheral aryl groups.

We also calculated the optimized geometry of the compound with a m-Cl aryl group as seen in the minor (11%) disordered component (Fig. S6 in the Supporting Information); the optimized structure also similarly showed the intramolecular H-bond, and was only 0.92 kcal/mol higher in energy when compared with the p-Cl isomer. Our subsequent discussions will thus focus on only the major p-Cl isomer.

2.2.2. Potential energy surface (PES) scans

We scanned the potential energy surface (PES) of the (TPP)Rh (PhNHOH)(C_6H_4Cl-p) compound to examine the energetic preference of the intramolecular H-bonding interaction. Specifically, we rotated the hydroxyl O–H bond around the C–N–O fragment by varying the

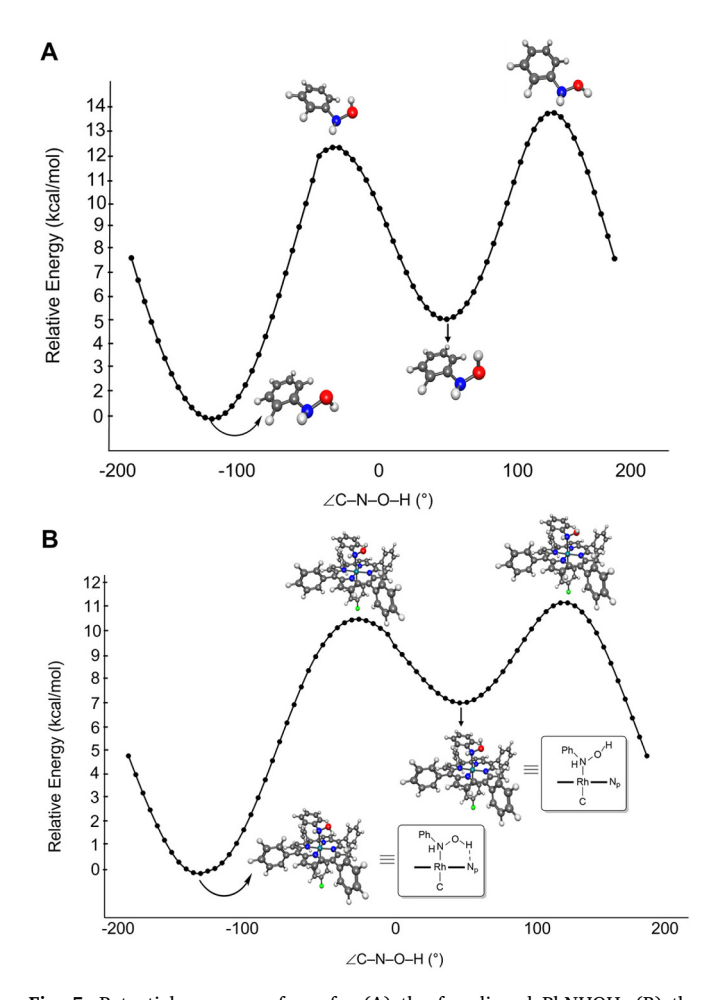


Fig. 5. Potential energy surfaces for (A) the free ligand PhNHOH, (B) the complex (TPP)Rh(PhNHOH)($C_6H_4Cl_-p$) from $\omega B97X-D/6-31+G^*$ calculations. The hydroxylamine C–N–O fragment was held intact while rotating the C–N–O–H dihedral angle in 5° increments over the full 360° range; the geometry at each constrained angle was reoptimized and the single-point energy calculated.

hydroxylamine \angle C-N-O-H dihedral angle in stepwise increments of 5° (Fig. 5) from -180° to $+180^{\circ}$. Geometry optimization of the structure was performed with the dihedral angle constrained at each value, and the single-point energy of the system was recorded. We performed the PES scans of different –NHOH conformations for both the free PhNHOH ligand and the adduct (TPP)Rh(PhNHOH)(C₆H₄Cl-p).

The PES scan for the unbound PhNHOH molecule is shown in Fig. 5A, and reveals two energy minima. The global energy minimum displays a "pointing down" conformation of the –NHO \underline{H} proton (\angle C–N–O–H = –120°). The alternate local minimum "pointing up" conformation is 5.35 kcal/mol higher in energy. When bound to the Rh center (Fig. 5B), this "pointing down" orientation preference is maintained (\angle C–N–O–H = –130°) to allow the –NHO \underline{H} proton to engage in an intramolecular H-bond with the porphyrin N atom. In the case of the Rh complex (Fig. 5B), this "down" (global minimum) conformation is 7.10 kcal/mol lower in energy than the corresponding "up" (local minimum) conformation. Taking into account the contribution of the ligand conformational energies (Fig. 5A), the contribution of (TPP)Rh(C₆H₄Cl) fragment to this overall stabilization of the "down" conformation is thus calculated to be 1.75 kcal/mol.

2.2.3. Natural bond orbital (NBO) analysis

We utilized second-order perturbative analysis [34] on the optimized structure of (TPP)Rh(PhNHOH)(C_6H_4Cl-p), to elucidate the contributing

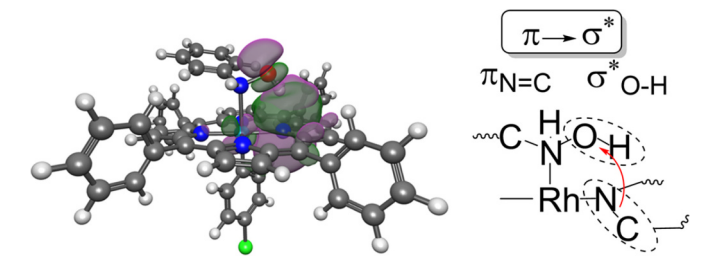


Fig. 6. NBO plot of (TPP)Rh(PhNHOH)(C_6H_4Cl) showing the interaction between the donor π N=C (por) and acceptor σ^* O–H at the ω B97X-D/LANL2DZ/6–31+G* level of theory. The top view of the porphyrin showing the isolated donor π N=C (por) orbital is depicted for additional clarity in Fig. S15A.

molecular orbital interactions involved in the binding of the axial PhNHOH ligand that enabled the intramolecular H-bonding feature. Selected results are shown in Fig. 6. In addition to the primary N-donor interaction of PhNHOH to the Rh center (lone pair donation from axial N to Rh) of 19.59 kcal/mol (first entry of Table 1), a secondary π (N=C of porphyrin) to the σ^* antibonding orbital of the hydroxylamine NHO–H moiety of 2.32 kcal/mol was found. Similarly, the π - σ^* interaction for the (disordered) m-Cl aryl isomer was found to be 2.30 kcal/mol.

Importantly, this 2.32 kcal/mol binding contribution of the intramolecular H-bond to the overall interaction of PhNHOH to the "(TPP)Rh (C_6H_4Cl-p)" fragment is lower than that previously determined by us for AmphNHOH in a six-coordinate Fe porphyrin (3.04 kcal/mol) but higher than that for a five-coordinate Co porphyrin (1.36 kcal/mol) [22]. We note that the latter two systems involved AmphNHOH which is an *alkyl*hydroxylamine. We have, to date, not been able to isolate a Rh porphyrin *alkyl*hydroxylamine complex, however. Consequently, we sought to determine computationally if there could be differences in the intramolecular H-bonding interactions that were dependent on the nature of the hydroxylamine (i.e., aryl vs. alkyl).

2.2.4. Metal-bound alkylhydroxylamines (RNHOH) versus arylhydroxylamines (ArNHOH)

We hypothesized that as the observed intramolecular H-bonding interaction involves a porphyrin $\pi \to \sigma^*$ (O–H) donor-acceptor interaction, that a relatively electron-rich *alkyl*hydroxylamine (RNHOH) should display the weaker $\pi \to \sigma^*$ interaction, and that the less electron-rich *aryl*hydroxylamine (ArNHOH) should enable a stronger $\pi \to \sigma^*$ interaction with the same metalloporphyrin fragment (Fig. 7).

We optimized the structure of $(TPP)Rh(CH_3NHOH)(C_6H_4Cl-p)$ as a model alkylhydroxylamine complex. The optimized structure similarly revealed the presence of the intramolecular H-bonding interaction in the

 $\label{thm:condition} \textbf{Table 1} \\ \textbf{Natural Bond Orbital analysis results for different rhodium hydroxylamines and alkylaldoximes complexes using ωB97X-D functional, LANL2DZ/ECP.} \\$

Complexes ^a	Donor ^b	Acceptor ^b	Energy (kcal/mol)
Hydroxylamines			_
[Rh](PhNHOH)	π N7-C25	σ* O3–H4	2.32
	(LP) σ N9	d∗ Rh	19.59
[Rh](CH ₃ NHOH)	π N7-C25	σ* O3–H4	1.94
	(LP) σ N9	d∗ Rh	23.05
[Rh](CH ₃ (CH ₂) ₃ NHOH)	π N7-C25	σ* O3–H4	1.79
	(LP) σ N9	d∗ Rh	20.06
Oximes			
[Rh](CH ₂ =NOH)	π N7-C24	σ* O3–H4	2.11
	(LP) σ N9	d∗ Rh	21.61
$[Rh](Z-CH_3(CH_2)_2CH=NOH)$	π N40-C47	σ* O90–H91	1.88
	(LP) σ N89	d∗ Rh	21.91

^a [Rh] represents the five-coordinate (TPP)Rh(C₆H₄Cl-*p*) fragment.

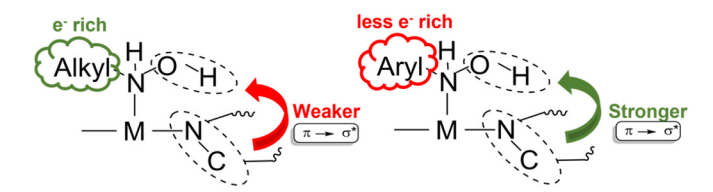


Fig. 7. Sketch of the porphyrin π -to- $\sigma^*(O-H)$ interaction.

global minimum structure (Supporting Information, Fig. S7). The results of our NBO analysis on the optimized structure revealed that the $\pi\to\sigma^*$ interaction contributed 1.94 kcal/mol to the overall binding of CH₃NHOH to the Rh porphyrin, which is lower than the 2.32 kcal/mol determined for the aryl PhNHOH analog described above, and consistent with our hypothesis in Fig. 7. In addition, the $\pi\to\sigma^*$ interaction, as determined by an NBO analysis, of the optimized structure of the related longer chain butylhydroxylamine (TPP)Rh(CH₃(CH₂)₃NHOH)(C₆H₄Cl-p) analogue was calculated at 1.79 kcal/mol, also consistent with our hypothesis. The latter model was computed for comparison with its oxime analogue (see next section). These and related NBO data are collected in Table 1.

2.2.5. Metal-bound alkylhydroxylamines (RNHOH) versus aldoximes (R'CH=NOH)

As mentioned in the Introduction, we are interested in determining whether the observed and (to date) rare intramolecular H-bonding feature in metalloporphyrin-alkyl/arylhydroxylamine complexes can extend to other *N*-bound ligands. Here, we extend our studies to include *N*-liganded oximes containing C=N(OH) double bonds (c.f., single C=N(OH) bonds in hydroxylamines and a change in formal hybridization of the N-atom that binds to the metal).

We computed the optimized geometry of the model formaldoxime complex (TPP)Rh(CH $_2$ =NOH)(C $_6$ H $_4$ Cl-p). The optimized structure similarly revealed the presence of the internal H-bond between the oxime C=NOH proton and a porphyrin N-atom (Supporting Information Fig. S8).

We then performed an NBO analyses on the (TPP)Rh(CH₂=NOH) (C_6H_4Cl -p) compound for comparison with the hydroxylamine model (TPP)Rh(CH₃NHOH)(C_6H_4Cl -p) described above. Two features regarding the comparison of Rh-bound CH₂=NOH and CH₃NHOH are evident (Fig. S9 in the Supporting Information and Table 1).

2.2.6. Isolation and DFT investigation of a rhodium porphyrin aldoxime complex

Experimentally, we had difficulty isolating and crystallizing a well-defined (TPP)Rh(aldoxime)(C₆H₄Cl) compound. After several unsuccessful attempts with other aldoximes (e.g., with acetaldoxime, α -benzaldoxime), we were fortunate to obtain suitable crystals of the n-butyraldoxime (TPP)Rh(CH₃(CH₂)₂CH=NOH)(C₆H₄Cl-p) derivative for a single-crystal X-ray diffraction study. This compound was obtained in 69% isolated yield from adduct formation of the aldoxime with the five-coordinate (TPP)Rh(C₆H₄Cl-p) precursor (bottom of Scheme 1) in a manner similar to that utilized for the PhNHOH compound (top of Scheme 1). The IR spectrum of the product as a KBr pellet displayed a band at 929 cm $^{-1}$ which we assign to ν_{NO} based on comparison with its computed spectrum (Figs. S10-S11 in the Supporting Information). The crystal structure of the product (TPP)Rh(CH₃(CH₂)₂CH=NOH)(C₆H₄Cl-

 $[^]b$ $\pi=$ bonding orbital; located on a porphyrin pyrrole N=C fragment. $\sigma^*=$ antibonding orbital; located on the hydroxyl OH group. Atom numbering refers to the calculated structures.

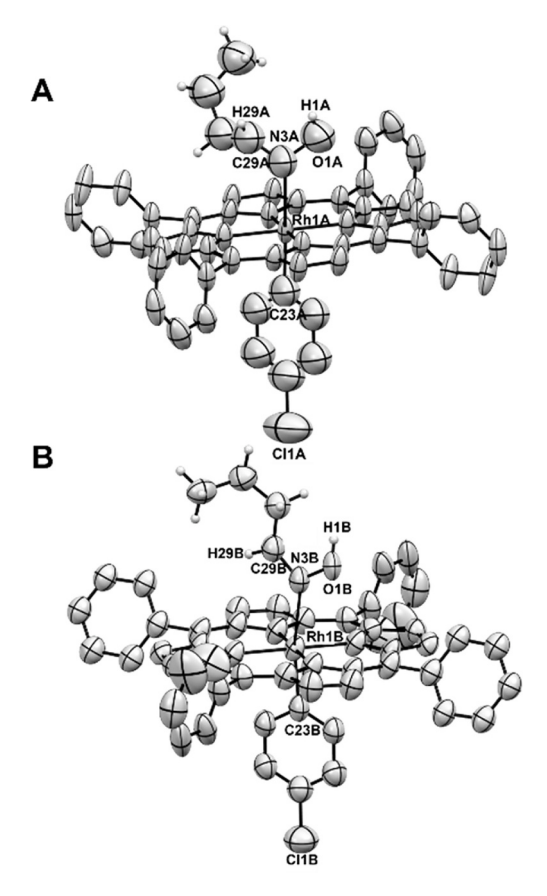


Fig. 8. Molecular structure of (A) E- and (B) Z-(TPP)Rh(CH $_3$ (CH $_2$) $_2$ CH=NOH) (C $_6$ H $_4$ Cl-p). The H atoms of the –NOH moieties in both isomers (A and B) were located by geometry and their positions were refined independently to verify the specific locations. Thermal ellipsoids are drawn at 50%.

p) is shown in Fig. 8, and reveals the presence of two molecules in a 1:1 ratio that correspond to the presence of the *E* (Fig. 8A) and *Z* (Fig. 8B) conformations of the oxime C–C=N–O moieties (right of Fig. 1), consistent with a general restricted rotation about the C=N double bond in this organic fragment.

The axial ligands in both these molecules are also disordered across their respective porphyrin planes. The H-atoms bonded to the aldoxime O-atoms were located by geometry, and their positions were refined independently to verify their specific locations. Selected geometrical data for the two molecules of (TPP)Rh(CH $_3$ (CH $_2$) $_2$ CH=NOH)(C $_6$ H $_4$ Cl- $_p$) are collected in Table 2.

Curiously, the oxime C=NOH protons in these structures were situated in an "up" conformation that did not position them for the anticipated intramolecular H-bonds with a porphyrin N-atom (Fig. 8, and Fig. S12 in the Supporting Information).

We note that several oxime-based ligands bound to rhodium (III)

Table 2 Selected bond lengths (Å) and angles ($^{\circ}$) for the structurally characterized (A) *E*-and (B) *Z*-(TPP)Rh(CH₃(CH₂)₂CH=NOH)(C₆H₄Cl-*p*) compounds.

	Molecule with E-oxime A	Molecule with Z-oxime B
Rh–N	2.281(13)	2.286(13)
Rh-C	1.982(16)	1.975(16)
N-O	1.418(14)	1.420(13)
C=N	1.320(16)	1.321(16)
∠Rh–N–O	122.1(8)	121.8(8)
$\angle Rh-N=C$	128.9(10)	129.7(9)
∠C=N - O	108.5(11)	108.3(11)
$\angle C$ - C = N - O	115(2)	3(2)

non-porphyrin complexes via N-atom have been well characterized by IR, ¹H NMR and X-ray crystallography, namely those with bidentate (e. g., amine-oxime) [35–40] and tetradentate (e.g., amine-oxime) [41,42] and imine-oxime [43] complexes. In each of these cases, the coordinated oxime-NOH moieties are intramolecularly H-bonded to each other through the oxime-H and the oximato-O atoms. Although the coordination chemistry of oximes, including multifunctional cyanoximes [44], is well-developed, we are not aware of crystal structural characterizations of heme models with neutral oxime ligands. In contrast, Fe porphyrins with *anionic* (i.e., deprotonated) "–ON=CR₂" fragments have been structurally characterized [45,46], and these contain the O-bound liganded forms.

Returning to the isolated and structurally characterized (TPP)Rh (CH₃(CH₂)₂CH=NOH)(C₆H₄Cl-p) in Fig. 8, we utilized DFT calculations to further probe the absence of the intramolecular bond in the X-ray structure. Geometry optimization of the complexes with the E- and Zoxime conformations, starting with the X-ray derived coordinates, reproduced both experimental X-ray structures quite well (Fig. S13 in the Supporting Information). The energy difference between the two calculated complexes with the Z- and the E-oxime conformations was \sim 1 kcal/mol (with the *E*-oxime slightly lower in energy). The largest deviations between the experimental and calculated structures (RMSD 0.3582 Å) of the complex with the E-oxime moiety were in the axial aldoxime and aryl ligands (Fig. S13A in the Supporting Information), whereas for the Z-oxime derivative the largest deviations (RMSD 0.3382) were in the porphyrin's peripheral aryl groups (Fig. S13B in the Supporting Information). Considering that our primary interest was in the axial aldoxime moiety, we focused our subsequent computations of the geometry optimized structure of the complex with the Z-oxime conformation.

A PES scan of the free *Z*-oxime ligand as a function of a change of the C=N-O-H torsion angle is shown in Fig. S14, whereas that for its complex with the Rh porphyrin is shown in Fig. 9. The energy difference between the local minimum with "H up" and the global minimum with "H down" is 6.95 kcal/mol in the free *Z*-oxime ligand (and 5.82 kcal/mol for the *E*-oxime; not shown), and 10.85 kcal/mol in the Rh complex for the *Z*-oxime. Overall, the energy stabilization of the H-down conformation to enable an intramolecular H-bond is calculated from the PES to be 3.90 kcal/mol.

The NBO plot showing the calculated $\pi \rightarrow \sigma^*$ interaction for geometry-optimized (TPP)Rh(CH₃(CH₂)₂CH=NOH)(C₆H₄Cl) at the global energy minimum, with the hypothetical intramolecular H-bond, is shown in Fig. 10. The calculated $\pi \rightarrow \sigma^*$ binding interaction was determined to be

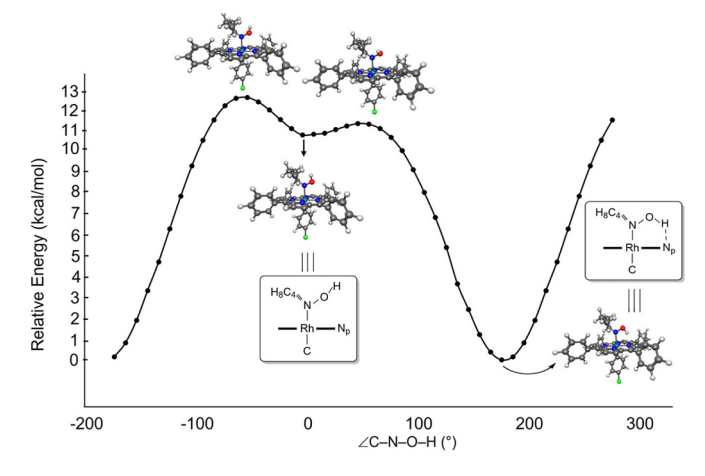


Fig. 9. Potential energy surfaces for the geometry optimized Z-(TPP)Rh (CH₃(CH₂)₂CH=NOH)(C₆H₄Cl-p) from ω B97X-D/LANL2DZ/6–31+G* calculations. The oxime C=N-O fragment was held intact while rotating the C=N-O-H dihedral angle in 5° increments over the full 360° range; the geometry at each constrained angle was reoptimized and the single-point energy calculated.

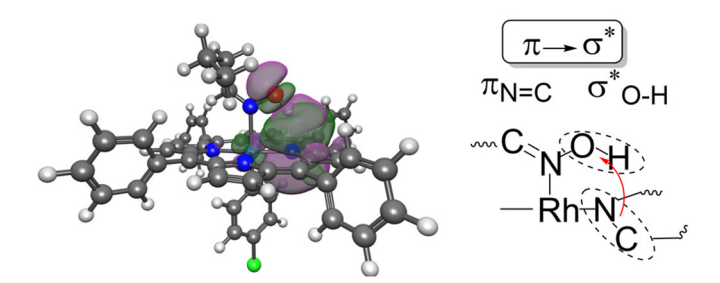


Fig. 10. NBO plot of the model Z-(TPP)Rh(CH₃(CH₂)₂CH=NOH)(C₆H₄Cl-p) compound showing the interaction between the donor π orbital (N40-C47) and acceptor σ^* orbital (O90-H91) at the ω B97X-D/LANL2DZ/6–31+G* level of theory. The top view of the porphyrin showing the donor π N=C (por) orbital is shown in Fig. S15C.

1.88 kcal/mol (bottom of Table 1) which is slightly lower than that previously described for the model Rh–CH $_2$ =NOH formaldoxime complex (at 2.11 kcal/mol) with a shorter carbon-chain. This calculated trend is not unexpected based on our discussions above regarding electron-richness of the axial ligand and its effect on the strength of the $\pi \to \sigma^*$ interactions.

Importantly, although DFT calculations predict the existence of an intramolecular H-bond for the aldoxime complex (TPP)Rh $(CH_3(CH_2)_2CH=NOH)(C_6H_4Cl-p)$, the experimental crystal structure obtained in this work (Fig. 8) revealed the absence of this H-bond. Rather, the structure was consistent with the conformation for the calculated *local* but not the *global* minimum of the *Z*-oxime ligand when in complex with the Rh porphyrin. We are unsure of the exact reason(s) for the inconsistency in the experimental versus calculated result for this isolated aldoxime derivative. A tempting but cautious scenario, out of several possibilities, is that we fortuitously accessed this local minimum H-up conformation in the selected crystal (out of a mixture) due to our crystallization conditions. We are continuing our efforts to obtain ordered and well-defined crystals of other aldoxime derivatives to further clarify the likelihood of this intramolecular H-bonding feature as determined for the isolated PhNHOH complex described in this paper.

3. Conclusions

Given that heme plays significant roles in the binding and metabolism of organic compounds containing the N-hydroxyl -NOH moiety, we sought to probe the fundamental nature of binding of such compounds with synthetic metalloporphyrins in the absence of competing Hbonding groups such as distal pocket residues and water. Specifically, and to expand this fundamental study to encompass both biological and non-biological metals, we sought to determine if an intramolecular Hbond, which we observed previously for alkylhydroxylamine derivatives of the first-row transition metals Fe and Co, would be present for an arylhydroxylamine and with a second-row transition metal. We demonstrate in this work that such an intramolecular H-bond, involving a (por) π -to- σ *(OH) donor-acceptor interaction, is present in the secondrow transition metal complex (TPP)Rh(PhNHOH)(C₆H₄Cl) containing an arylhydroxylamine. Results of DFT calculations, including a scan along the potential energy surface focused on the -NOH moiety, are consistent with the observation of the intramolecular H-bond in (TPP)Rh (PhNHOH)(C₆H₄Cl). This result suggests that, in the absence of

competing H-bond interactions in the vicinity of the hydroxylamine ligand (e.g., provided by some protein distal pockets and water), we cannot immediately rule out the participation of such intramolecular Hbonds in the binding and activation of R/ArNHOH molecules. In contrast, although DFT calculations suggest the existence of this intramolecular H-bond for the related aldoximes, the crystal structure we obtained for the butyraldoxime adduct (TPP)Rh(CH₃(CH₂)₂CH=NOH) (C₆H₄Cl-p) did not display this H-bond. Importantly, the crystal structures reported in this work are the first reports of isolation and structural characterization of any hydroxylamine or oxime ligand with a Rh porphyrin. We do note, however, that such internal H-bonds between ligands and heme pyrrole-N atoms in have not, to date, been reported in crystal structures of heme proteins. We are currently extending this work to other alkyl/arylhydroxylamines and aldoximes to explore the factors that lead to the experimental observations of such intramolecular H-bonds between the bound -NOH ligands and pyrrole-N atoms in synthetic metalloporphyrins.

4. Experimental

4.1. General

The reactions were performed under anaerobic conditions under an atmosphere of nitrogen using standard Schlenk techniques and/or in an Innovative Technology Labmaster 100 Dry Box unless stated otherwise. Phenylhydroxylamine (95%; Sigma-Aldrich) and butyraldoxime (95%; Tokyo Chemical Industry (TCI)), and (TPP)Rh(C₆H₄Cl) (Frontier Scientific, batch: JY09–2714; TPP = tetraphenylporphyrin dianion) were purchased from commercial suppliers. Solvents used for the reactions (CH₂Cl₂, hexane) were obtained from an Innovative Technology Pure Solv 400–5-MD Solvent Purification system under an atmosphere of nitrogen. A Bio-Rad FT-155 FTIR spectrometer was used to record the infrared spectra.

4.2. $(TPP)Rh(PhNHOH)(C_6H_4Cl)$

In a Schlenk tube, (TPP)Rh(C₆H₄Cl) (8.5 mg, 0.010 mmol) was dissolved in CH₂Cl₂ (4 mL) with constant stirring. Excess phenylhydroxylamine (7.1 mg, 0.065 mmol) was then added to the stirred solution, and the reaction left to stir for 3 h, during which time the color of the solution changed from dark orange-red to a vibrant pink-purple color. The solution was taken to dryness in vacuo and the residue was redissolved in CH₂Cl₂ (2 mL). Slow evaporation of this CH₂Cl₂/hexane (2:1) solution in a glove box resulted in the formation of red block-shaped crystals. The crystals were isolated and the air-sensitive product identified as (TPP)Rh(PhNHOH)(C₆H₄Cl) (5.9 mg, 0.0061 mmol, \sim 61% isolated yield) by X-ray crystallography. IR (KBr, cm $^{-1}$): υ_{NO} = 1074 m; also 3450 s, 3261 m, 1598 m, 1538 w, 1440 m, 925 m, 796 s, 752 s, 701 s.

4.3. $(TPP)Rh(CH_3(CH_2)_2CH=NOH)(C_6H_4Cl-p)$

Excess butyraldoxime (18 mg (0.02 mL), 0.21 mmol) was added into a stirred CH₂Cl₂ solution of (TPP)Rh(C₆H₄Cl-p) (10 mg, 0.012 mmol), and the reaction left to stir overnight (~12 h), during which time the color of the solution changed from red-pink to a scarlett red color. The solution was taken to dryness in vacuo and 5 mL of hexane was added. The suspension was vigorously stirred for 15 min, then the solvent was decanted and the residue was further dried under vacuum. Slow evaporation of this CH₂Cl₂/pentane (2:1) solution in a glove box resulted in the formation of red plate-shaped crystals. The crystals were isolated product and the air-sensitive identified (TPP)Rh $(CH_3(CH_2)_2CH=NOH)(C_6H_4Cl-p)$ (7.6 mg, 0.0083 mmol, ~67% isolated yield) by X-ray crystallography. IR (KBr, cm $^{-1}$): $v_{NO} = 929$ m; also 3395 s, 2961 s, 2932 w, 2874 w, 1660 w, 1596 m, 1382 w, 1011 s, 795 s, 748 s, 699 s.

 $^{^1\,}$ For example, the experimental IR spectrum of the product as a KBr pellet displays a notable band in the $3200\text{--}3600~\text{cm}^{-1}$ region (Fig. S10A in the Supporting Information); the calculated spectrum of the "H up" conformer of the complex (Fig. S10C) only has a very weak band in this region, whereas that of the "H down" conformer (Fig. S10E) has an intense band in this region, suggestive of a mixture of the "H up" and H down" conformers in the experimental sample.

A comment on bulk sample purity: In this work, we focused on obtaining diffraction-quality single crystals for X-ray crystallography to probe the –NOH conformations and orientations. We have not been able, to date, to obtain reproducible ¹H NMR spectroscopy data for these two compounds, probably due to the presence of minor paramagnetic impurities in the bulk samples resulting from decomposition and/or further reactivity of the complexes. CHN elemental analyses to differentiate the target RNHOH versus the more stable RNO derivatives (i.e., addition/removal of two protons) is likely to be unreliable for these unstable compounds especially given the discussions dealing with reliability of current outsourced CHN determinations [47]. We note that the reported (porphyrin)Fe(*i*-PrNHOH)(*i*-PrNO) [23] and (porphyrin)Ru(PhNHOH) (PhNO) [24] compounds are also unstable in solution, resulting in the chemical conversion of the RNHOH groups to other moieties.

4.4. Computational details

All quantum mechanical (QM) electronic ground-state calculations were performed using the density functional theory (DFT) method [48,49]. Version 5.0 of the Q-Chem software package [50] was used, with IQmol as the visualization package. Molecular geometry optimization and energy studies were carried out using the ω B97X-D functional [51] and LANL2DZ effective core potential [52] (for Rh) and 6–31+G* basis set [53,54] (for the non-Rh atoms). The functional/basis set that best reproduced the experimental values from the X-ray structures was ω B97X-D as functional and LANL2DZ/6–31+G* as basis set, giving a good balance between reliability and computational speed. Once the ground-state geometry was obtained, the PES-SCAN, NBO analysis and vibrational frequencies were carried out for the different complexes.

Author statement

The manuscript was written through the contributions of all authors. All authors have approved the final version of the manuscript.

Declaration of Competing Interest

The authors declare that they have no known competing financial interests or personal relationships that could have appeared to influence the work reported in this paper.

Data availability

Data will be made available on request.

Acknowledgements

This material is based upon work supported by (while GBR-A was serving at) the U.S. National Science Foundation (NSF; CHE-2154603 and CHE-1900181). YS is supported by NSF Grant No. CHE-2102071. Any opinions, findings, and conclusions or recommendations expressed in this material are those of the authors and do not necessarily reflect the views of the NSF. We are grateful to the NSF MRI program (CHE-0130835) for funds to purchase the X-ray diffractometer. The graphical abstract was created with BioRender.com.

Appendix A. Supplementary data

Crystallographic data have been deposited with the CCDC (2,208,710 and 2,208,711) and can be obtained free of charge via www.ccdc.cam.ac.uk/data_request/cif. The Supporting Information contains experimental and computational details, and additional figures and tables. Supplementary data to this article can be found online at [https://doi.org/10.1016/j.jinorgbio.2023.112337].

References

- P. Cedervall, A.B. Hooper, C.M. Wilmot, Structural studies of hydroxylamine oxidoreductase reveal a unique heme cofactor and a previously unidentified interaction partner, Biochemistry 52 (2013) 6211–6218.
- [2] M.A. Smith, S.H. Majer, A.C. Vilbert, K.M. Lancaster, Controlling a burn: outer-sphere gating of hydroxylamine oxidation by a distal base in cytochrome P460, Chem. Sci. 10 (2019) 3756–3764.
- [3] J. Kostera, J. McGarry, A.A. Pacheco, Enzymatic interconversion of ammonia and nitrite: the right tool for the job, Biochemistry 49 (2010) 8546–8553.
- [4] O. Einsle, A. Messerschmidt, R. Huber, P.M.H. Kroneck, F. Neese, Mechanism of the six-electron reduction of nitrite to ammonia by cytochrome c nitrite reductase, J. Am. Chem. Soc. 124 (2002) 11737–11745.
- [5] A. Dietl, C. Ferousi, W.J. Maalcke, A. Menzel, S. de Vries, J.J. Keltjens, M.S. Jetten, B. Kartal, T.R. Barends, The inner workings of the hydrazine synthase multiprotein complex, Nature 527 (2015) 394–397.
- [6] S. Nakano, M. Takahashi, A. Sakamoto, H. Morikawa, K. Katayanagi, The reductive reaction mechanism of tobacco nitrite reductase derived from a combination of cystal structures and ultraviolet-visible microspectroscopy, Proteins Struct. Funct. Genet. 80 (2012) 2035–2045.
- [7] K. Fukuyama, T. Okada, Structures of cyanide, nitric oxide and hydroxylamine complexes of Arthromyces ramosus peroxidase at 100 K refined to 1.3 angstrom resolution: coordination geometries of the ligands to the haem iron, Acta Crystallogr. D 63 (2007) 472–477.
- [8] B.N. Brown, K.J. Robinson, Q.C. Durfee, D. Kekilli, M.A. Hough, C.R. Andrew, Hydroxylamine complexes of cytochrome c': influence of heme iron redox state on kinetic and spectroscopic properties, Inorg. Chem. 59 (2020) 14162–14170.
- [9] V.M. Florence, E.W. Di Stefano, C.Y. Sum, A.K. Cho, The metabolism of (R)-(-)-amphetamine by rabbit liver microsomes: initial products, Drug Metab. Dispos. 10 (1982) 312–315.
- [10] A.H. Beckett, P.M. Belanger, Metabolic incorporation of oxygen into primary and secondary aliphatic-amines and consequences in carbon-nitrogen bond-cleavage, J. Pharm. Pharmacol. 27 (1975) 547–552.
- [11] M. Kiese, The biochemical production of ferrihemoglobin-forming derivatives from aromatic amines, and mechanisms of ferrihemoglobin formation, Pharmacol. Rev. 18 (1966) 1091–1161.
- [12] J.N. Burstyn, M. Iskandar, J.F. Brady, J.M. Fukuto, A.K. Cho, Comparative studies of N-hydroxylation and N-demethylation by cytochrome P-450, Chem. Res. Toxicol. 4 (1991) 70–76.
- [13] M. Kiese, Significance of the oxidation of aniline to nitrosobenzene for the formation of methemoglobin after absorption of aniline into the organism, Arch. Exp. Pathol. Pharmakol. 235 (1959) 360–364.
- [14] M. Sørenson, E.H.J. Neilson, B.L. Møller, Oximes: unrecognizedd chameleons in general and specialized plant metabolism, Mol. Plant 11 (2018) 95–117.
- [15] K.-I. Oinuma, Y. Hashimoto, K. Konishi, M. Goda, T. Noguchi, H. Hiashibata, M. Kobayashi, Novel aldoxime dehydratase involved in carbon-nitrogen triple bond synthesis of *Pseudomonas chloraraphis* B23, J. Biol. Chem. 278 (2003) 29600–29608.
- [16] Y. Asano, Y. Kato, Z-Phenylacetaldoxime degradation by a novel aldoxime dehydratase from Bacillus sp. strain OxB-1, FEMS Microbiol. Lett. 158 (1998) 185–100.
- [17] Y. Kato, K. Nakamura, H. Sakiyama, S.G. Mayhew, Y. Asano, Novel heme-containing lyase, phenylacetaldoxime dehydratase from *Bacillus* sp. strain OxB-1: purification, characterization, and molecular cloning of the gene, Biochemistry 39 (2000) 800–809.
- [18] K. Chen, Z. Wang, K. Ding, Y. Chen, Y. Asano, Recent progress on discovery and resaerch of aldoxime dehydratases, Green Synth. Catal. 2 (2021) 179–186.
- [19] H. Sawai, H. Sugimoto, Y. Kato, Y. Asano, Y. Shiro, S. Aono, X-ray crystal structure of Michaelis complex of aldoxime dehydratase, J. Biol. Chem. 284 (2009) 32089–32096.
- [20] D. Matsui, N. Muraki, K. Chen, T. Mori, A.A. Ingram, K. Oike, H. Groger, S. Aono, Y. Asano, Crystal structural analysis of aldoxime dehydratase from *Bacillus* sp. OxB-1: importance of surface residues in optimization for crystallization, J. Inorg. Biochem. 230 (2022), 111770.
- [21] K. Kobayaahi, S. Yoshioka, Y. Kato, Y. Asano, S. Aono, Regulation of aldoxime dehydratase activity by redox-dependent change in the coordination structure of the aldoxime-heme complex, J. Biol. Chem. 280 (2005) 5486–5490.
- [22] Y. Guan, J. Londoño-Salazar, Z. Pei, D.R. Powell, Y. Shao, G.B. Richter-Addo, Interactions of N-hydroxyamphetamine with an iron porphyrin: a unique intramolecular H-bond probed by DFT calculations, J. Inorg. Biochem. 231 (2022), 111779.
- [23] D. Mansuy, P. Battioni, J.-C. Chottard, C. Riche, A. Chiaroni, Nitrosoalkane complexes of iron-porphyrins: analogy between the bonding properties of nitrosoalkanes and dioxygen, J. Am. Chem. Soc. 105 (1983) 455–463.
- [24] J.-L. Liang, J.-S. Huang, Z.-Y. Zhou, K.-K. Cheung, C.-M. Che, Interaction between dioxoruthenium(VI) porphyrins and hydroxylamines: coordination of N-substituted hydroxylamine to ruthenium and X-ray crystal structures of ruthenium complexes with a unidentate nitrosoarene ligand, Chem. Eur. J. 7 (2001) 2306–2317.
- [25] B. Wang, C. Li, K.D. Dubey, S. Shaik, Quantum mechanical/molecular mechanical calculated reactivity networks reveal how cytochrome P450cam and its T252A mutant select their oxidation pathway, J. Am. Chem. Soc. 137 (2015), 7379-7390 (Fig. S20).
- [26] M. Altarsha, T. Benighaus, D. Kumar, W. Thiel, How is the reactivity of cytochrome P450cam affected by Thr252X mutation? A QM/MM study for X = Serine, Valine, Alanine, Glycine, J. Am. Chem. Soc. 131 (2009) 4755–4763 (Figs S5, S8–9, S18, S221.

- [27] D. Luckhaus, The rovibrational spectrum of hydroxylamine: a combined high resolution experimental and theoretical study, J. Chem. Phys. 106 (1997) 8409–8426
- [28] R. Withnall, L. Andrews, Matrix infrared spectra and normal-coordinate analysis of isotopic hydroxylamine molecules, J. Phys. Chem. 92 (1988) 2155–2161.
- [29] M.N. Hughes, K. Shrimanker, Metal complexes of hydroxylamine, Inorg. Chim. Acta 18 (1976) 69–76.
- [30] J. Olguin, H. Muller-Bunz, M. Albrecht, Springloaded porphyrin NHC hybrid rhodium(III) complexes: carbene dissociation and oxidation catalysis, Chem. Commun. 50 (2014) 3488–3490.
- [31] T. Ikeda, M. Asakawa, M. Goto, K. Miyake, T. Ishida, T. Shimizu, STM observation of alkyl-chain-assisted self-assembled monolayers of pyridine-coordinated porphyrin rhodium chlorides, Langmuir 20 (2004) 5454–5459.
- [32] Y.Y. Qian, K.S. Chan, Base-promoted aryl carbon-iodine and carbon-bromine bond cleavage with rhodium porphyrin complexes: scope and mechanism, Organometallics 31 (2012) 5452–5462.
- [33] J.P. Collman, R. Boulatov, Aromatic and benzylic C-H bond activation in the system Bis(dicarbonylrhodium(I))-porphyrinate-hydrocarbon solvent, Inorg. Chem. 40 (2001) 2461–2464.
- [34] A.E. Reed, L.A. Curtiss, F. Weinhold, Intermolecular interactions from a natural bond orbital, donor-acceptor viewpoint, Chem. Rev. 88 (1988) 899–926.
- [35] G.E. Efe, E.O. Schlemper, Rhodium(III) complexes of new N-substituted alphaamine oxime ligands: synthesis and crystal structures of [Rh(phenao)₂Cl₂], [Rh (phetao)₂Cl₂], [Rh(acetanilidoao)₂Cl₂] and [Rh(N-methylacetanilidoao)₂Cl₂], Polyhedron 11 (1992) 2447–2458.
- [36] G.E. Efe, M.R.A. Pillai, E.O. Schlemper, D.E. Troutner, Rhodium complexes of two bidentate secondary amine oxime ligands and applications to the labelling of proteins, Polyhedron 10 (1991) 1617–1624.
- [37] N.R. Palepu, S. Adhikari, R. Premkumar, A.K. Verma, S.L. Shepherd, R.M. Phillips, W. Kaminsky, M.R. Kollipara, Half-sandwich ruthenium, rhodium and iridium complexes featuring oxime ligands: structural studies and preliminary investigation of in vitro and in vivo anti-tumour activities, Adv. Organomet. Chem. 31 (2017), e3640.
- [38] R. Acharyya, F. Basuli, G. Rosair, S. Bhattacharya, Synthesis, structure and electrochemical properties of some oxime complexes of rhodium, New J. Chem. 28 (2004) 115–119.
- [39] S. Siripaisarnpipat, E.O. Schlemper, Dinuclear rhodium(III) complexes: synthesis and crystal and molecular structures of two amine-oxime complexes of rhodium (III), Inorg. Chem. 22 (1983) 282–286.
- [40] R. Dreos, G. Tauzher, S. Geremia, L. Randaccio, F. Asaro, G. Pellizer, C. Tavanacco, G. Costa, An unusual reaction of bis(dimethylglyoximato) complexes: synthesis and

- characterization of rhodium(III) complexes containin an oxime-imine equatorial moiety, Inorg. Chem. 33 (1994) 5404–5410.
- [41] S. Siripaisampipat, E.O. Schlemper, Preparation, spectra, and crystal structures of two rhodium(III) complexes with short intramolecular hydrogen bonds, Inorg. Chem. 23 (1984) 330–334.
- [42] T. Lynde-Kernell, E.O. Schlemper, Preparation, characterization and crystal structures of two amine-oxime rhodium complexes, J. Coord. Chem. 16 (1988) 347-356
- [43] M. Moszner, M. Kubiak, J.J. Z, New rhodium complexes of the tetradentate ligand bis(diacetylmonoxime-imino)propane 1,3 (H₂dopn): synthesis and crystal structure of trans-[Rh(Hdopn)Cl]₂ and trans-[Rh(Hdopn)(I)₂], Inorg. Chim. Acta 357 (2004) 115–124.
- [44] N. Gerasimchuk, Chemistry and applications of cyanoximes and their metal complexes, Dalton Trans. 48 (2019) 7985–8013.
- [45] C.C.-Y. Wang, D.M. Ho, J.T. Groves, Models of nitric oxide synthase: Iron(III) porphyrin-catalyzed oxidation of fluorenone oxime to nitric oxide and fluorenone, J. Am. Chem. Soc. 121 (1999) 12094–12103.
- [46] D.S. Bohle, B.J. Conklin, C.-H. Hung, Coordination chemistry of the pseudochalcogen nitrite analog nitrosodicyanomethanide, Inorg. Chem. 34 (1995) 2569–2581
- [47] A. Katnelson, When do standards of chemical purity break down? Chem. Eng. News 101 (Issue 20) (2023). American Chemical Society, https://cen.acs.org/analytica l-chemistry/standards-chemical-purity-break-down/101/i110.
- [48] R.G. Parr, W. Yang, Density-Functional Theory of Atoms and Molecules, Oxford University Press, Place Published, 1989.
- [49] A.D. Becke, J. Chem. Phys. 140 (2014) 18A301.
- [50] E. Epifanovsky, et al., Software for the frontiers of quantum chemistry: an overview of developments in the Q-Chem 5 package, J. Chem. Phys. 155 (2021) 084801–084859
- [51] J.-D. Chai, M. Head-Gordon, Long-range corrected hybrid density functionals with damped atom-atom disperson corrections, Phys. Chem. Chem. Phys. 10 (2008) 6615–6620.
- [52] P.J. Hay, W.R. Wadt, Ab initio effective core potentials for molecular calculations. Potentials for main group elements Na to Bi, J. Chem. Phys. 82 (1985) 299–310.
- [53] W.J. Hehre, R. Ditchfield, J.A. Pople, Self-consistent molecular orbital methods. XII. Further extensions to Gaussian-type basis sets for use in molecular orbital studies of organic molecules, J. Chem. Phys. 56 (1972) 2257–2261.
- [54] P.C. Hariharan, J.A. Pople, The influence of polarization functions on molecular orbital hydrogenation energies, Theor. Chim. Acta 28 (1973) 213–222.